Photophysical Studies of a Room Temperature Phosphorescent Cd(II) based MOF and its Application towards Ratiometric Detection of Hg^{2+} Ions in Water

Prakash Majee,[a] Debal Kanti Singha,[a,b] Pooja Daga,[a] Sayani Hui,[b] Partha Mahata[b*] and Sudip Kumar Mondal[a*]

[a]Department of Chemistry, Siksha-Bhavana, Visva-Bharati University, Santiniketan-731235, West Bengal, India. Email: sudip.mondal@visva-bharati.ac.in

[b]Department of Chemistry, Jadavpur University, Jadavpur, Kolkata-700 032, West Bengal, India. Email: parthachem@gmail.com

ELECTRONIC SUPPLEMENTARY INFORMATION

* Corresponding Authors, E-mail: sudip.mondal@visva-bharati.ac.in, parthachem@gmail.com

Table S1: Selected bond distances (Å) observed in [Cd($C_5N_1S_1H_4$)($C_6O_5H_3$)], **Cd_1**.

Bond	Distances, Å	Bond	Distances, Å
Cd(1)-O(1)	2.303(3)	Cd(1)-O(2)	2.623(4)
Cd(1)-O(3)#1	2.335(3)	Cd(1)-S(1)	2.5417(10)
Cd(1)-O(4)#1	2.411(3)	Cd(1)-S(1)#2	2.7194(10)

Symmetry transformations used to generate equivalent atoms: #1 x-1/2,-y+1/2,z-1/2 #2 x+1,y,z

Table S2: Selected bond angles observed in [Cd($C_5N_1S_1H_4$)($C_6O_5H_3$)], **Cd_1**.

Angle	Amplitude (º)	Angle	Amplitude (º)
O(1)-Cd(1)-O(3)#1	122.35(11)	O(4)#1-Cd(1)-O(2)	102.79(11)
O(1)-Cd(1)-O(4)#1	152.32(12)	S(1)-Cd(1)-O(2)	147.10(7)
O(3)#1-Cd(1)-O(4)#1	55.54(10)	O(1)-Cd(1)-S(1)#2	77.98(8)
O(1)-Cd(1)-S(1)	94.68(8)	O(3)#1-Cd(1)-S(1)#2	134.21(8)
O(3)#1-Cd(1)-S(1)	121.62(9)	O(4)#1-Cd(1)-S(1)#2	87.05(8)
O(4)#1-Cd(1)-S(1)	109.47(8)	S(1)-Cd(1)-S(1)#2	93.34(3)
O(1)-Cd(1)-O(2)	52.45(10)	O(2)-Cd(1)-S(1)#2	81.86(8)
O(3)#1-Cd(1)-O(2)	82.12(10)		

Symmetry transformations used to generate equivalent atoms: #1 x-1/2,-y+1/2,z-1/2 #2 x+1,y,z

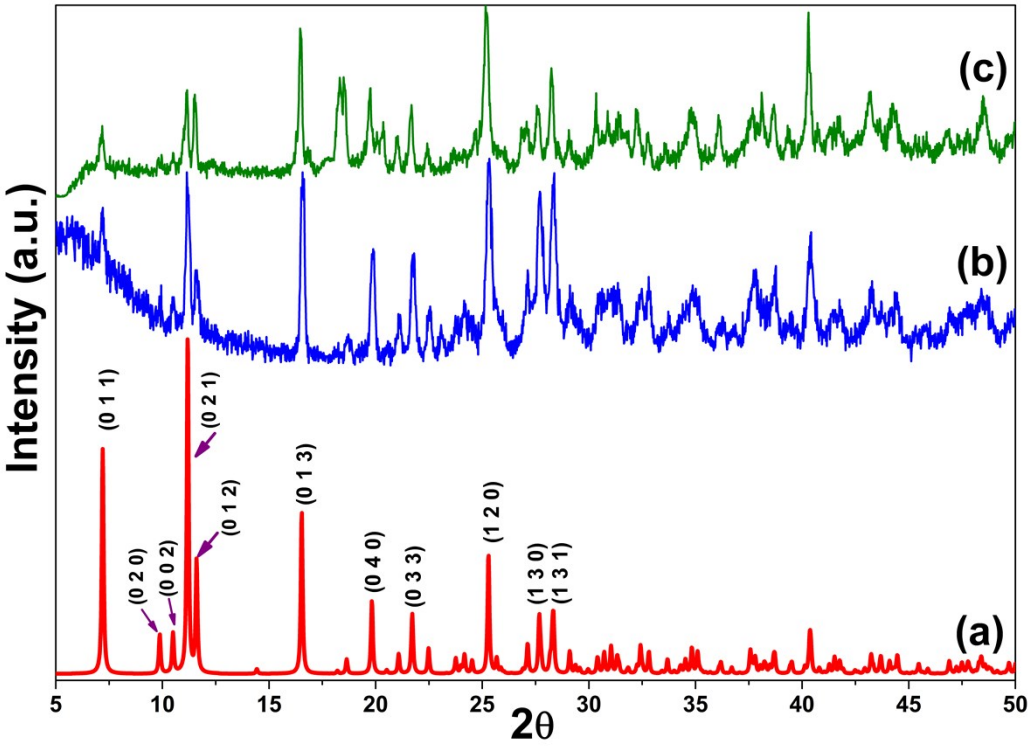

Fig. S1: Powder XRD (CuKα) patterns of $[Cd(C_5N_1S_1H_4)(C_6O_5H_3)]$, **Cd_1**: (a) simulated pattern from single crystal X-ray data (b) experimental data (c) after immerging in Hg^{2+} for 24 hours.

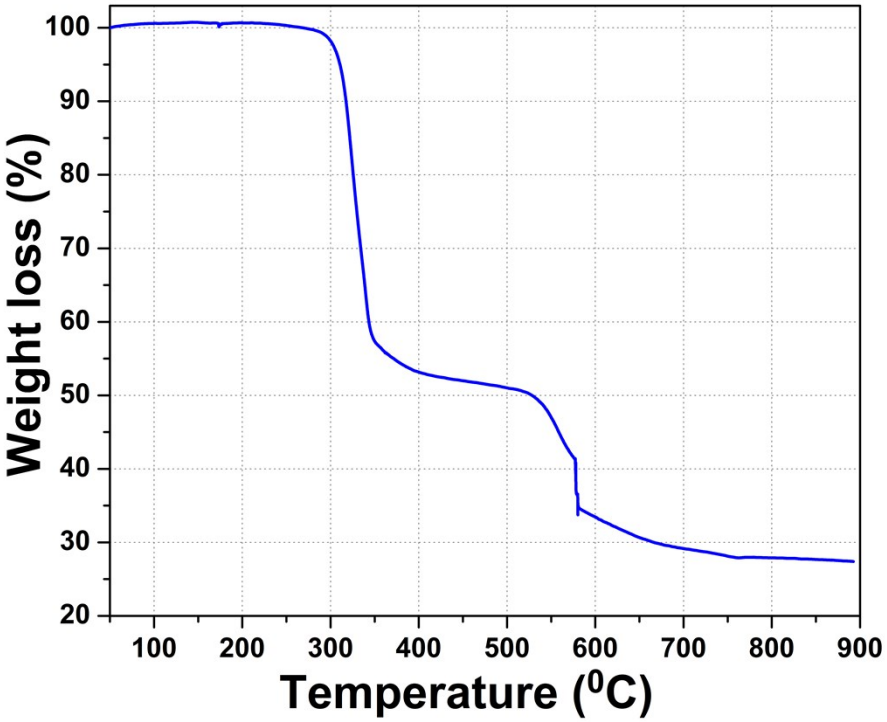

Fig. S2: Thermogravimetric analysis (TGA) of [Cd($C_5N_1S_1H_4$)($C_6O_5H_3$)], **Cd_1,** in nitrogen atmosphere.

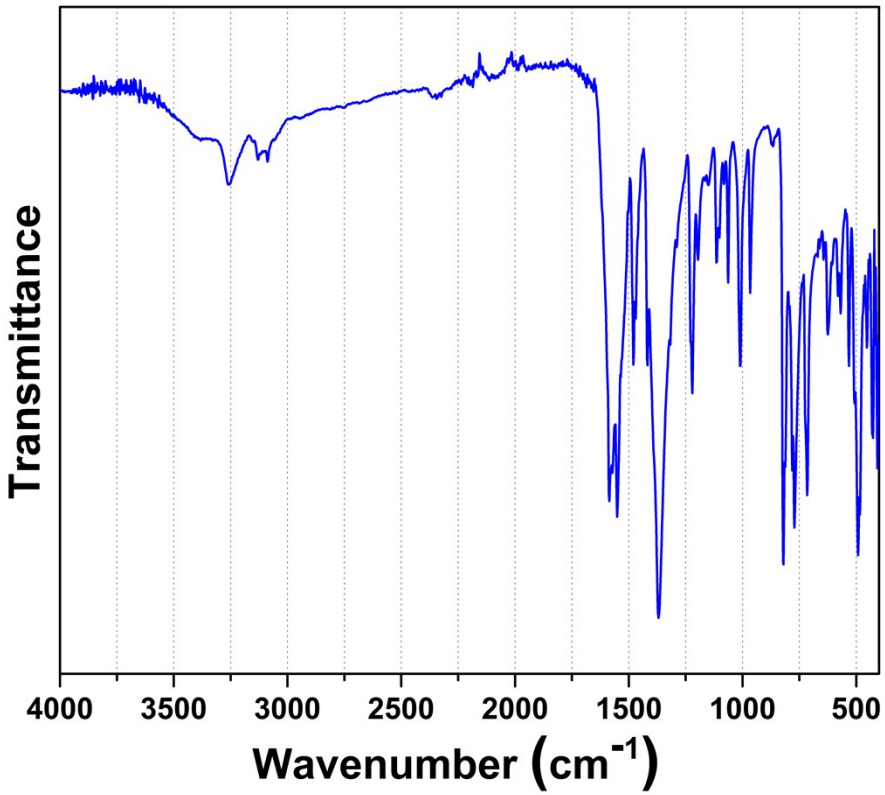

Fig. S3: IR spectrum of $[Cd(C_5N_1S_1H_4)(C_6O_5H_3)]$, **Cd_1.**

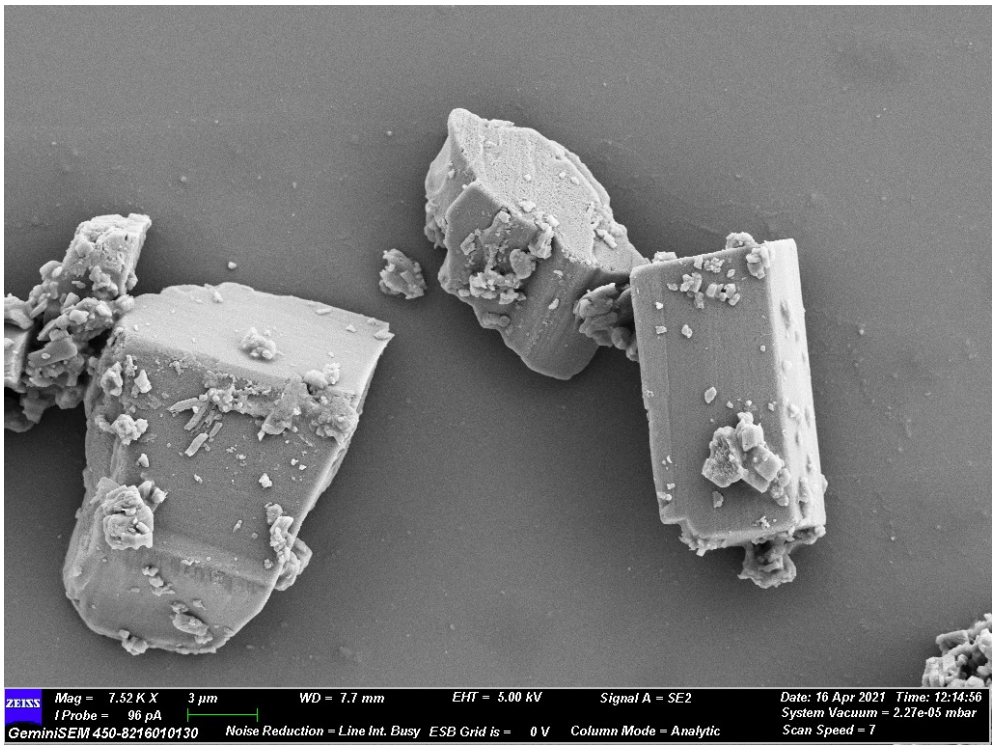

Fig. S4: SEM image of $[Cd(C_5N_1S_1H_4)(C_6O_5H_3)]$, **Cd_1.**

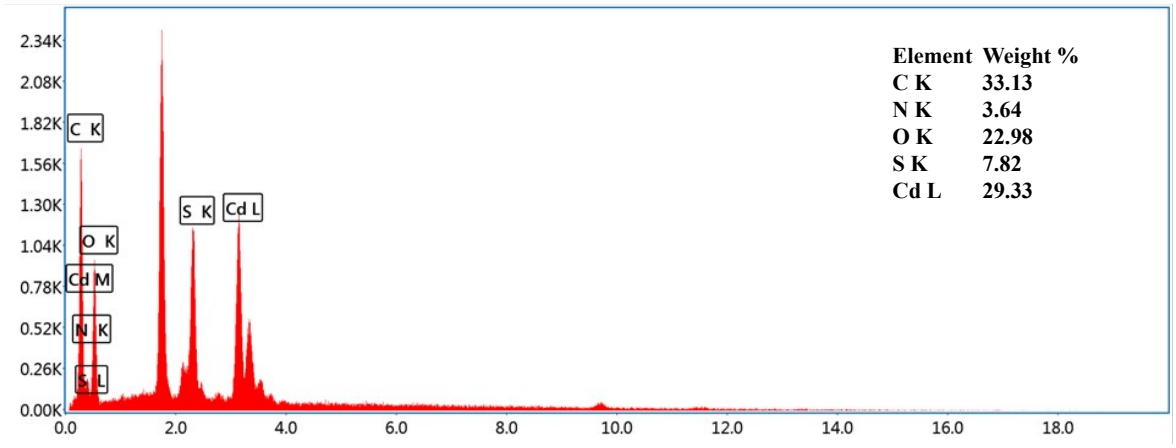

Fig. S5: Representative EDX plot of [Cd($C_5N_1S_1H_4$)($C_6O_5H_3$)], **Cd_1.**

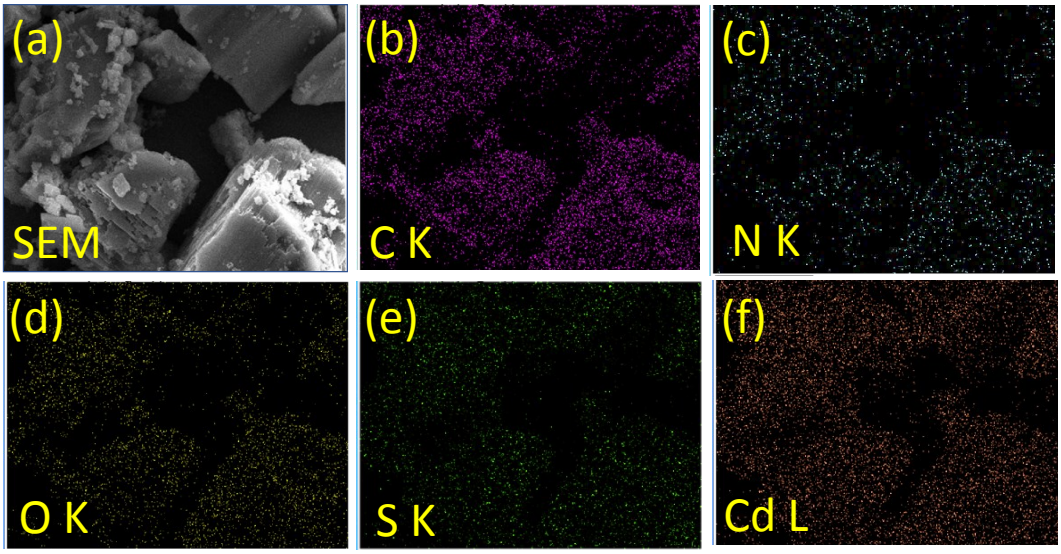

Fig. S6: (a) SEM image in which elemental mapping is performed in **Cd_1** and elemental mapping images, (b) C K, (c) N K, (d) O K (e) S K and (f) Cd L**.**

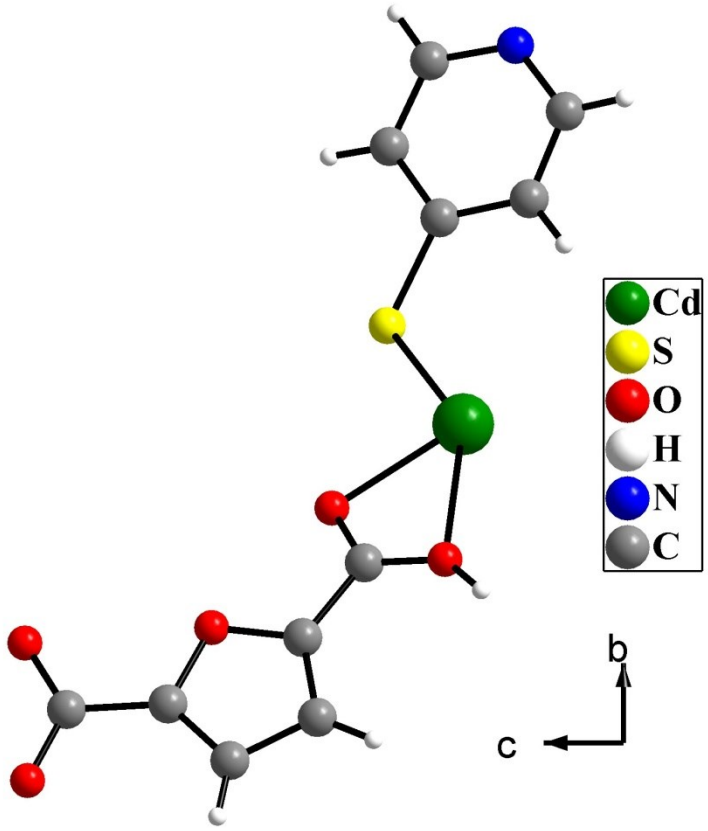

Fig. S7: Figure shows asymmetric unit of [Cd($C_5N_1S_1H_4$)($C_6O_5H_3$)], **Cd_1**.

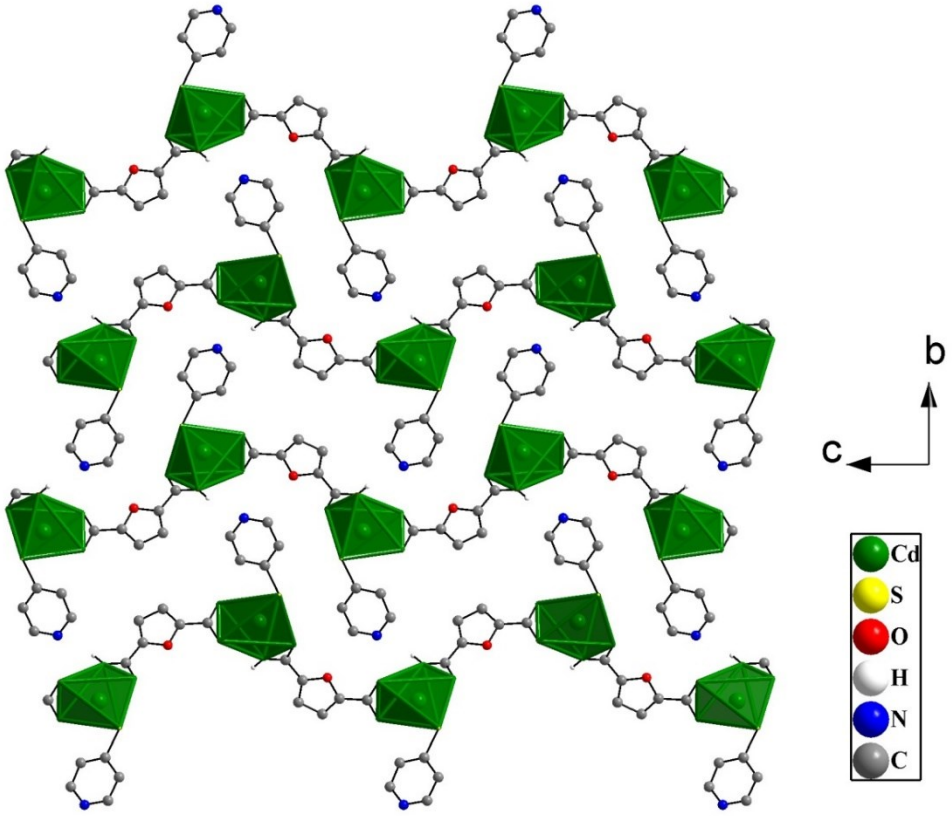

Fig. S8: Figure shows arrangement of the two-dimensional structures in *ABAB*….fashion in $[Cd(C_5N_1S_1H_4)(C_6O_5H_3)]$, **Cd_1**.

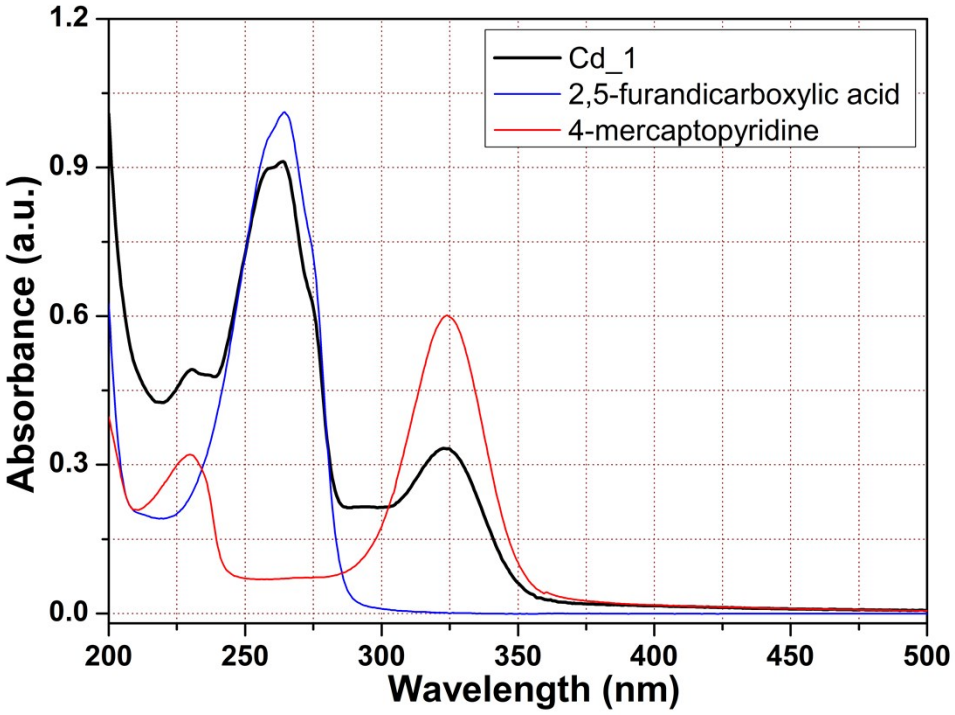

Fig. S9: Absorption spectra of compound **Cd_1** and corresponding ligands (furan-2,5-dicarboxylic acid and aldrithiol-4). The absorption band at ~ 325 nm which get diminished with the gradual addition of Hg^{2+} ions, is actually originated from the mercaptopyridine (4MPyH) moiety. The band (~325 nm) is most probably due to the n–π* (HOMO to LUMO) transition (non-bonding electron of pyridine N get excited to the π* orbital of ring carbon). With the addition of Hg^{2+} the non-bonding electrons of pyridine N get involved in the interaction with Hg^{2+} ions. As a result, the n–π* transition (~325 nm) get diminished. This is also a clear indication that the Hg^{2+} ions interacts with the N atom of pyridine moiety.

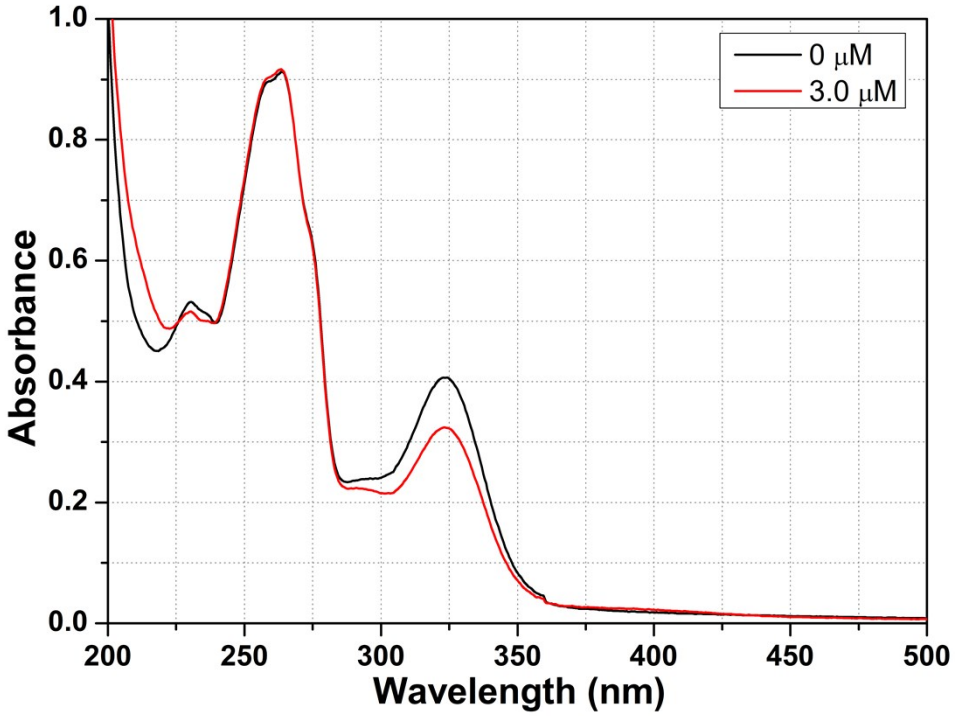

Fig. S10: Absorption of compound **Cd_1** and changes in spectra after the addition of Pb^{2+} (3 μM).

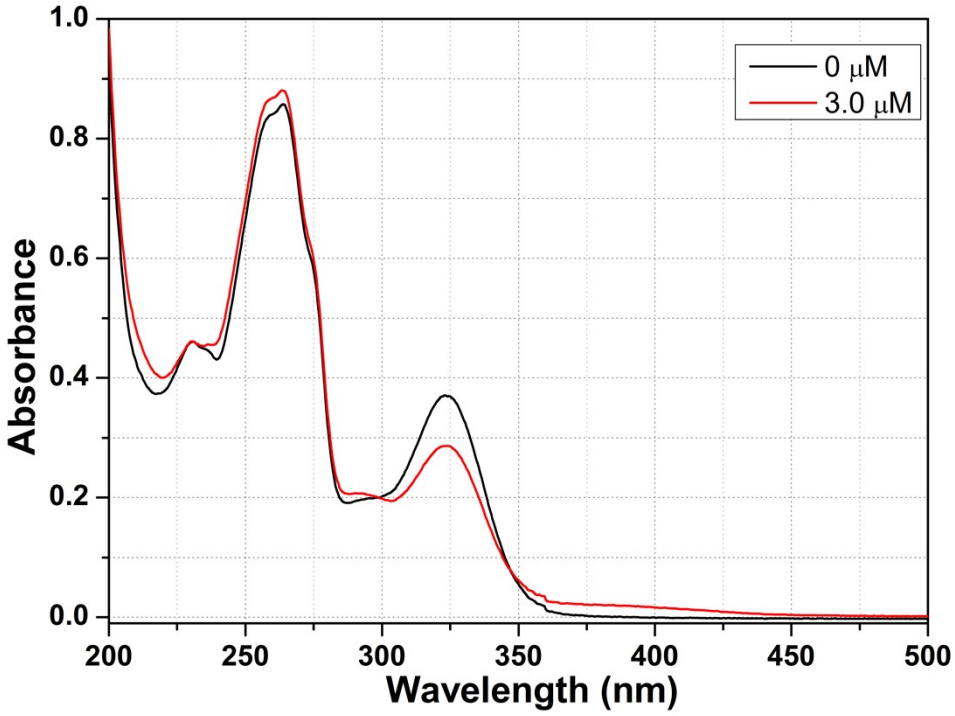

Fig. S11: Absorption of compound **Cd_1** and changes in spectra after the addition of Cu^{2+} (3 μM).

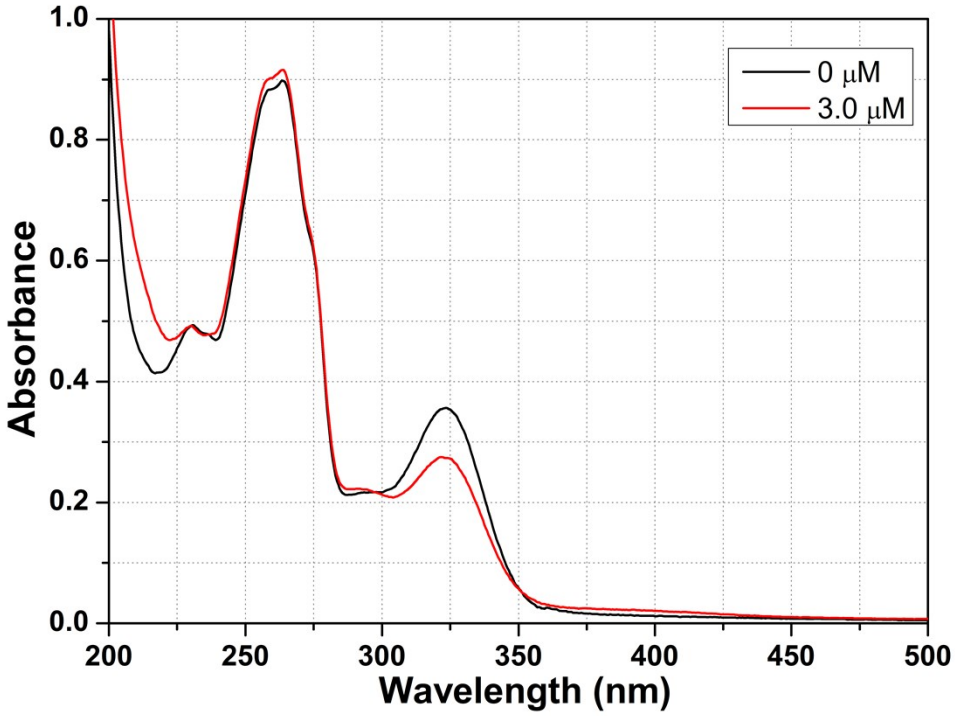

Fig. S12: Absorption of compound **Cd_1** and changes in spectra after the addition of Al^{3+} (3 μM).

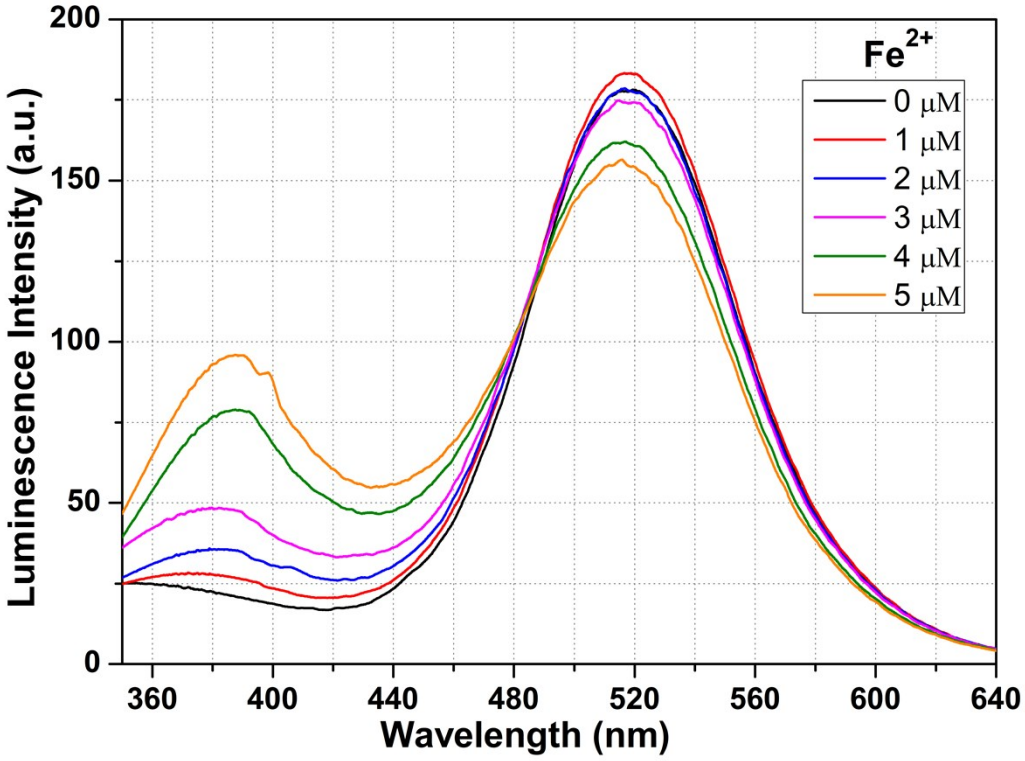

Fig. S13: Emission spectra of compound **Cd_1** dispersed in water upon incremental addition of Fe^{2+} solution (λ_{ex} = 330 nm). Final concentration of Fe^{2+} in the medium is indicated in the legend.

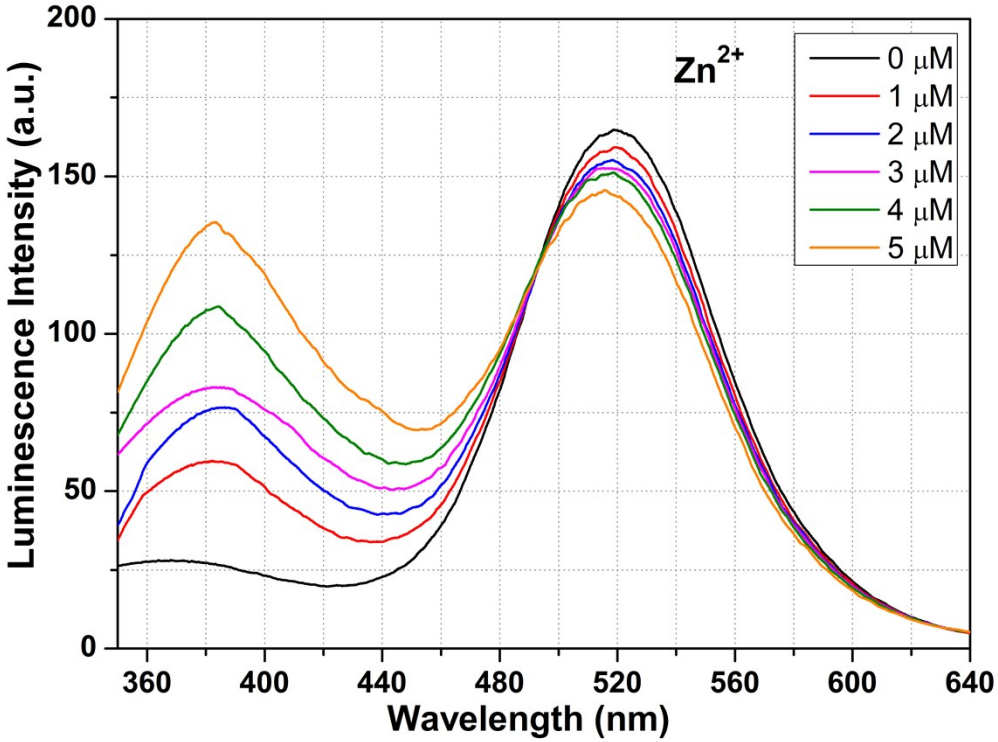

Fig. S14: Emission spectra of compound **Cd_1** dispersed in water upon incremental addition of Zn^{2+} solution (λ_{ex} = 330 nm). Final concentration of Zn^{2+} in the medium is indicated in the legend.

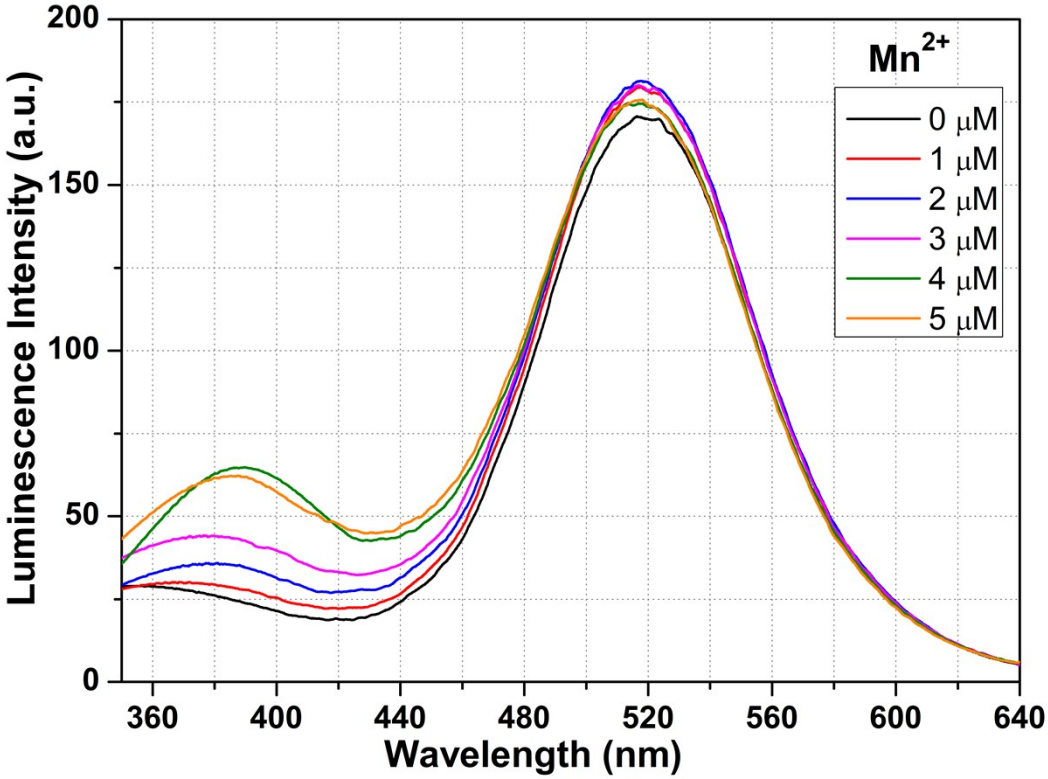

Fig. S15: Emission spectra of compound **Cd_1** dispersed in water upon incremental addition of Mn^{2+} solution (λ_{ex} = 330 nm). Final concentration of Mn^{2+} in the medium is indicated in the legend.

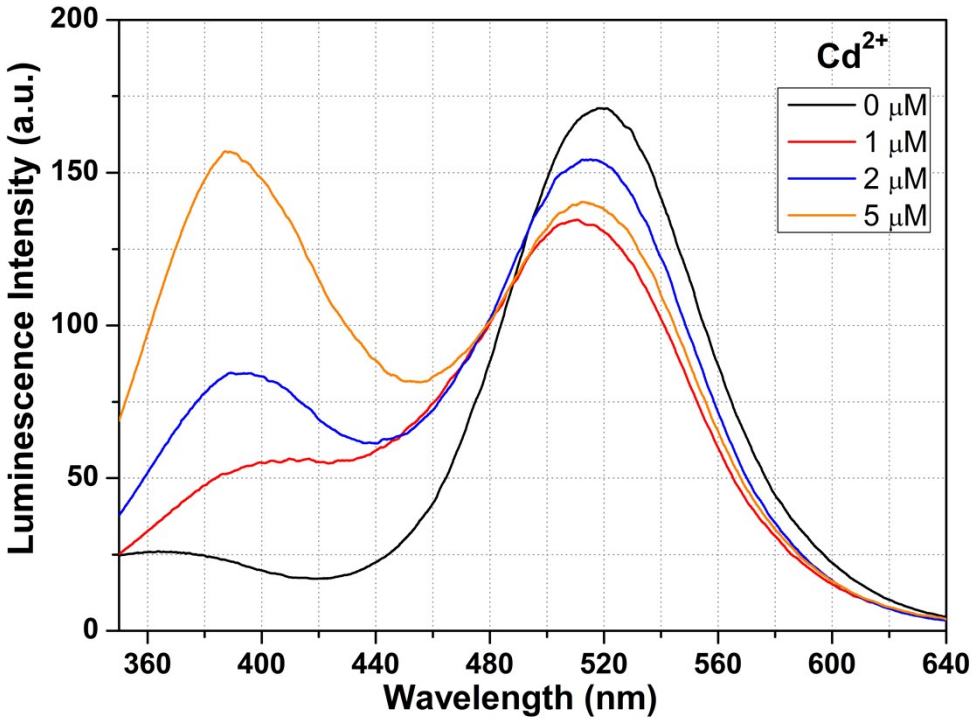

Fig. S16: Emission spectra of compound **Cd_1** dispersed in water upon incremental addition of Cd^{2+} solution (λ_{ex} = 330 nm). Final concentration of Cd^{2+} in the medium is indicated in the legend.

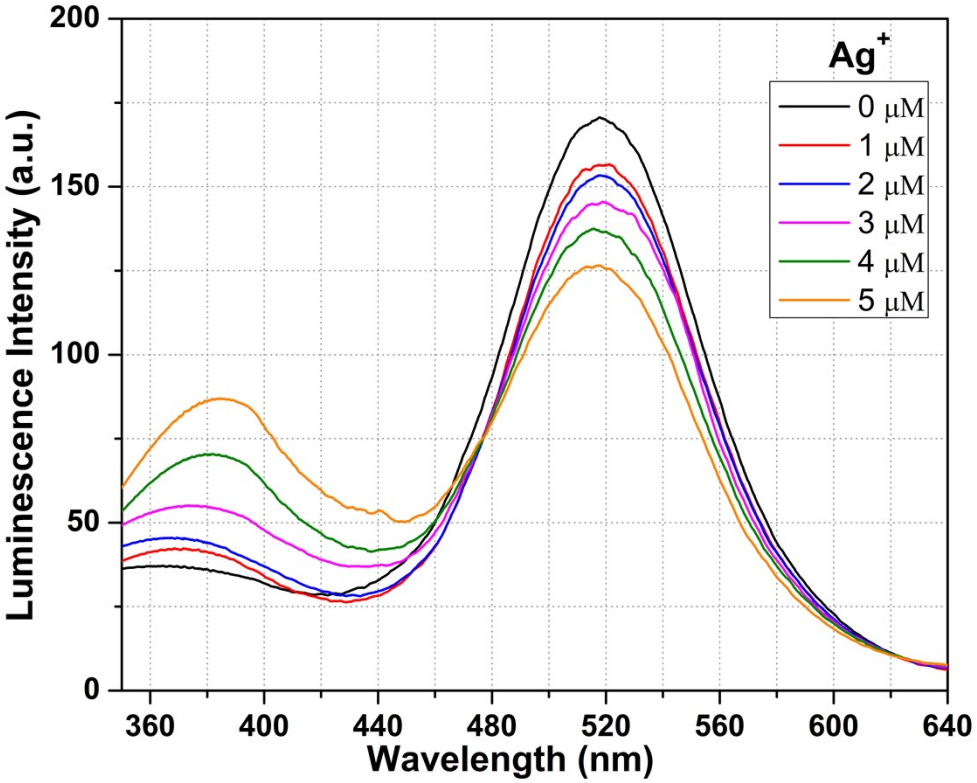

Fig. S17: Emission spectra of compound **Cd_1** dispersed in water upon incremental addition of Ag^+ solution (λ_{ex} = 330 nm). Final concentration of Ag^+ in the medium is indicated in the legend.

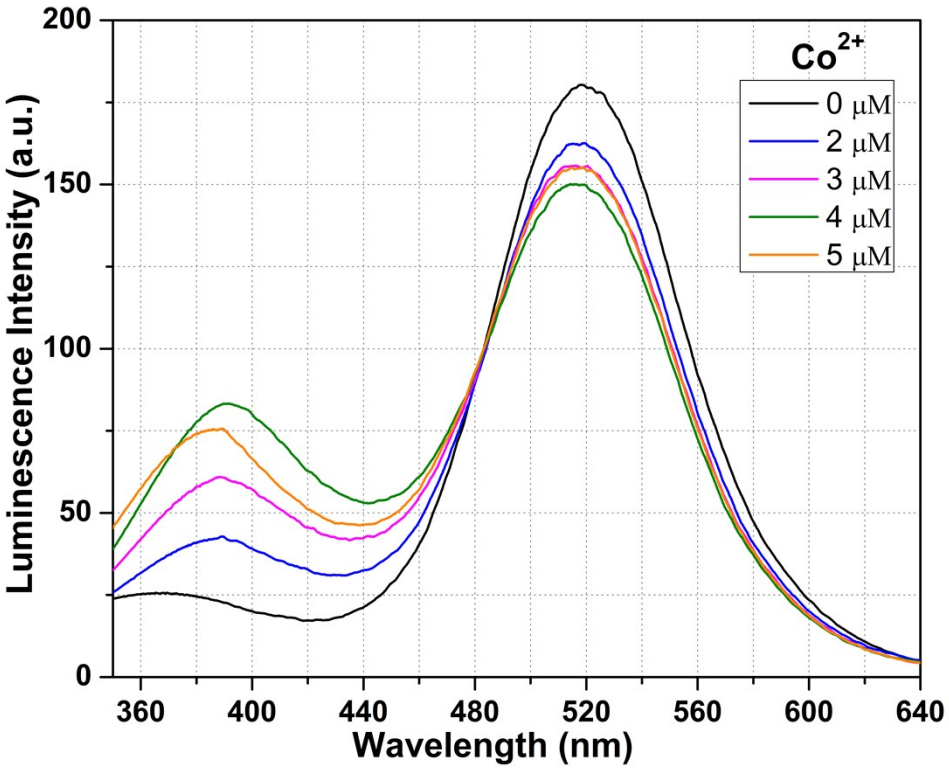

Fig. S18: Emission spectra of compound **Cd_1** dispersed in water upon incremental addition of Co^{2+} solution (λ_{ex} = 330 nm). Final concentration of Co^{2+} in the medium is indicated in the legend.

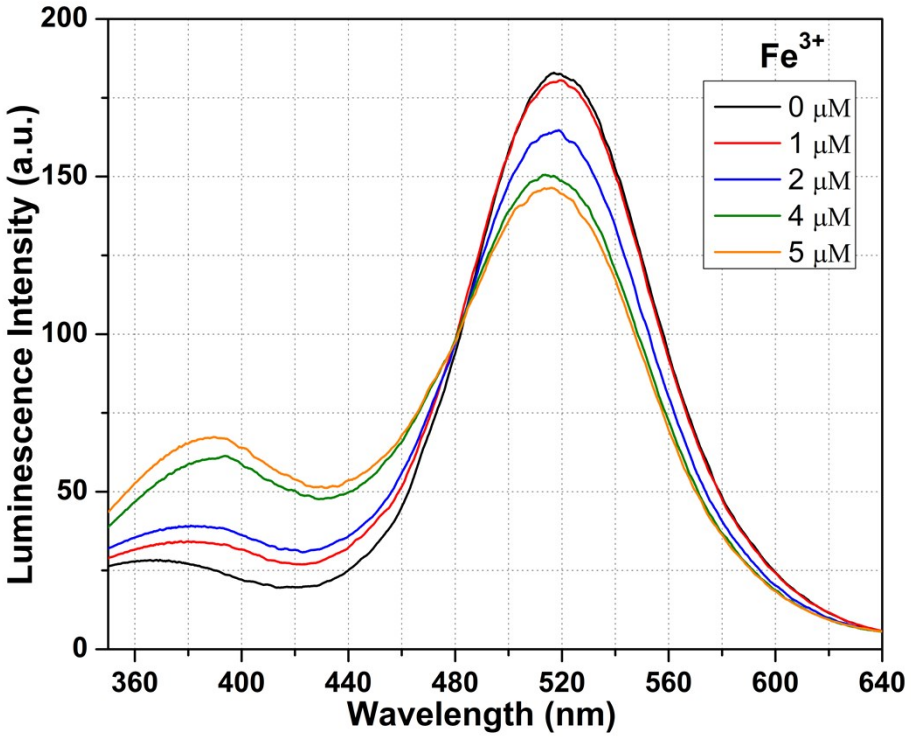

Fig. S19: Emission spectra of compound **Cd_1** dispersed in water upon incremental addition of Fe^{3+} solution (λ_{ex} = 330 nm). Final concentration of Fe^{3+} in the medium is indicated in the legend.

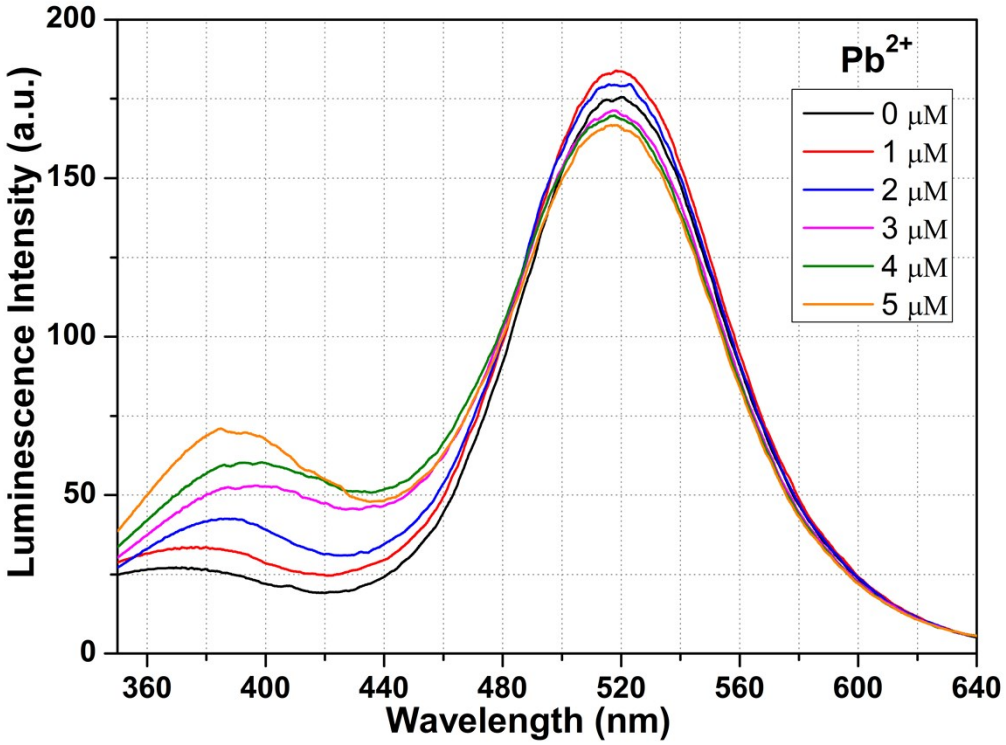

Fig. S20: Emission spectra of compound **Cd_1** dispersed in water upon incremental addition of Pb^{2+} solution (λ_{ex} = 330 nm). Final concentration of Pb^{2+} in the medium is indicated in the legend.

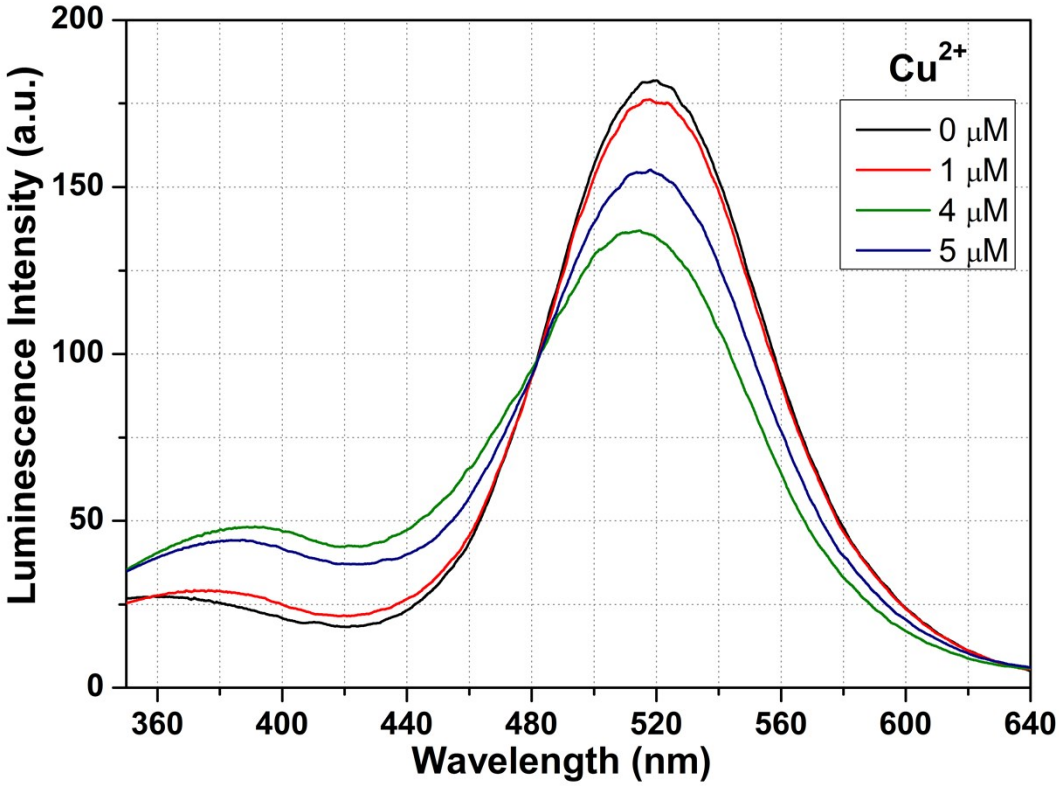

Fig. S21: Emission spectra of compound **Cd_1** dispersed in water upon incremental addition of Cu^{2+} solution (λ_{ex} = 330 nm). Final concentration of Cu^{2+} in the medium is indicated in the legend.

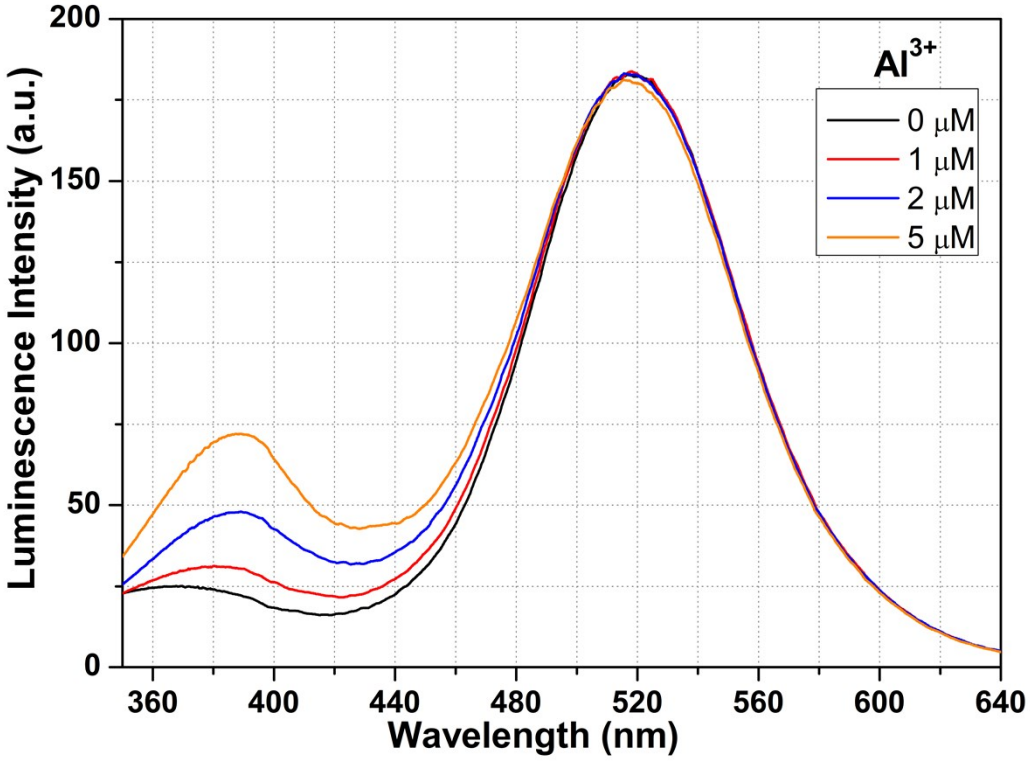

Fig. S22: Emission spectra of compound **Cd_1** dispersed in water upon incremental addition of Al^{3+} solution (λ_{ex} = 330 nm). Final concentration of Al^{3+} in the medium is indicated in the legend.

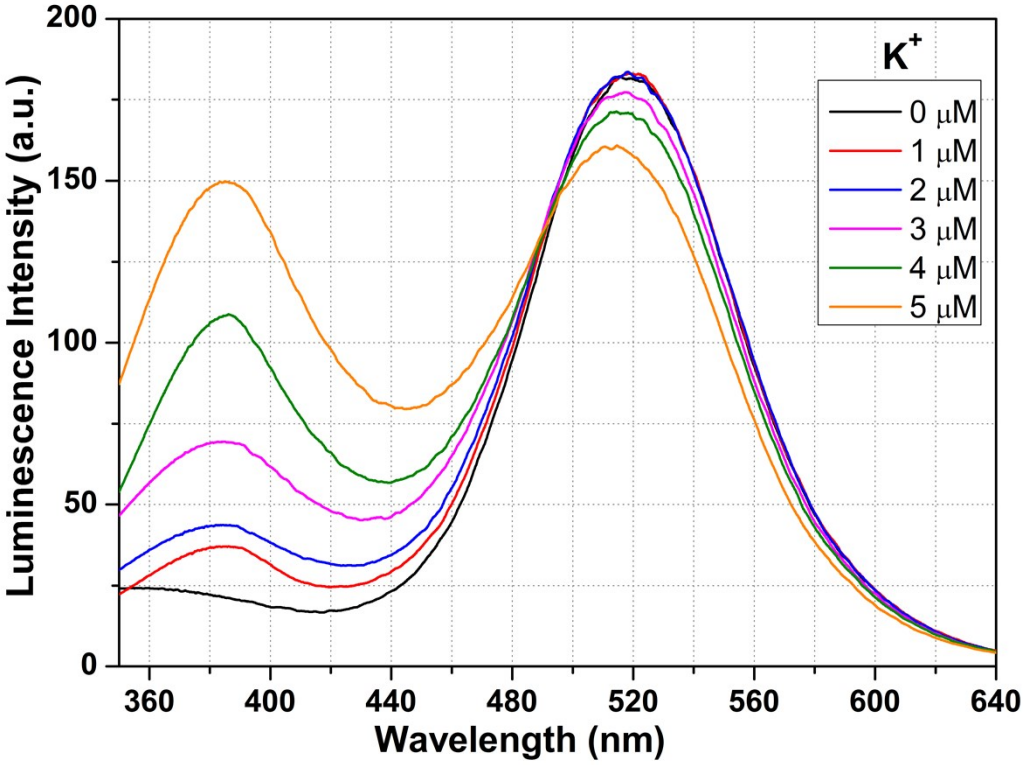

Fig. S23: Emission spectra of compound **Cd_1** dispersed in water upon incremental addition of K^+ solution (λ_{ex} = 330 nm). Final concentration of K^+ in the medium is indicated in the legend.

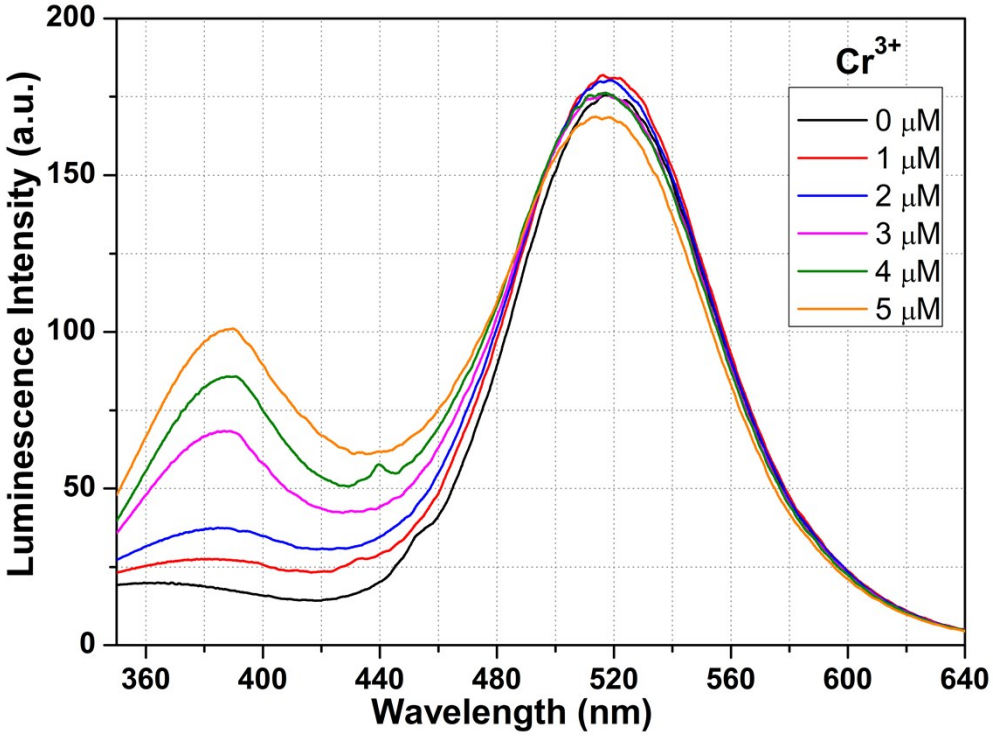

Fig. S24: Emission spectra of compound **Cd_1** dispersed in water upon incremental addition of Cr^{3+} solution (λ_{ex} = 330 nm). Final concentration of Cr^{3+} in the medium is indicated in the legend.

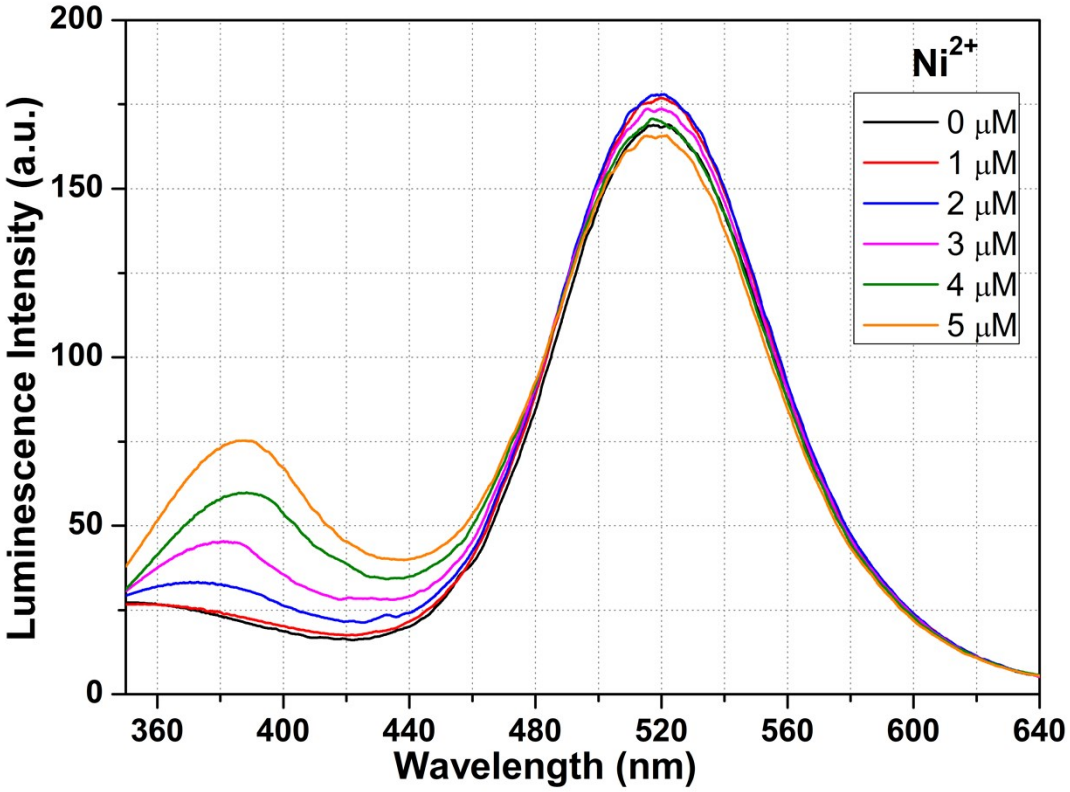

Fig. S25: Emission spectra of compound **Cd_1** dispersed in water upon incremental addition of Ni^{2+} solution (λ_{ex} = 330 nm). Final concentration of Ni^{2+} in the medium is indicated in the legend.

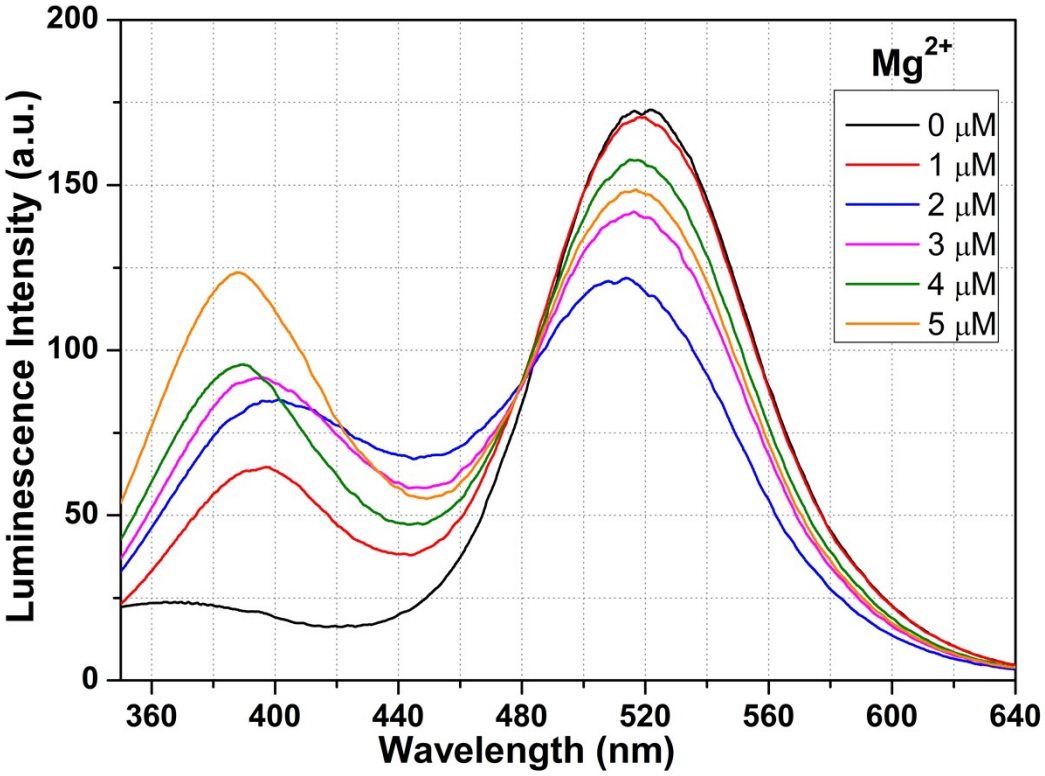

Fig. S26: Emission spectra of compound **Cd_1** dispersed in water upon incremental addition of Mg^{2+} solution (λ_{ex} = 330 nm). Final concentration of Mg^{2+} in the medium is indicated in the legend.

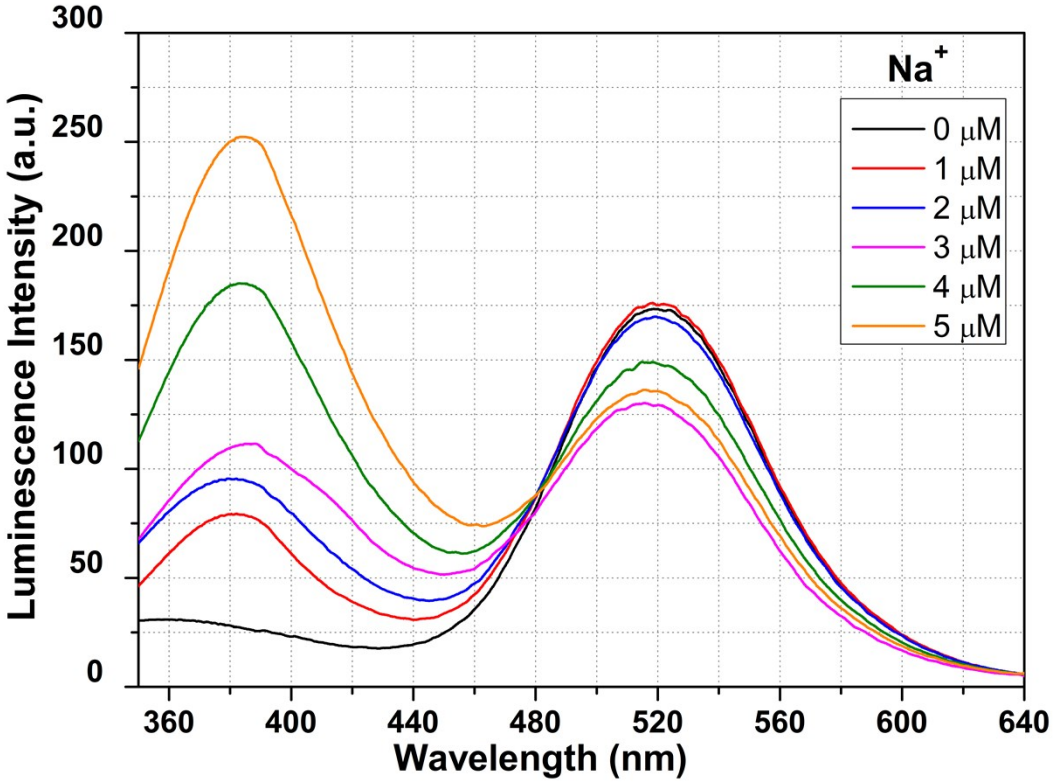

Fig. S27: Emission spectra of compound **Cd_1** dispersed in water upon incremental addition of Na^+ solution (λ_{ex} = 330 nm). Final concentration of Na^+ in the medium is indicated in the legend.

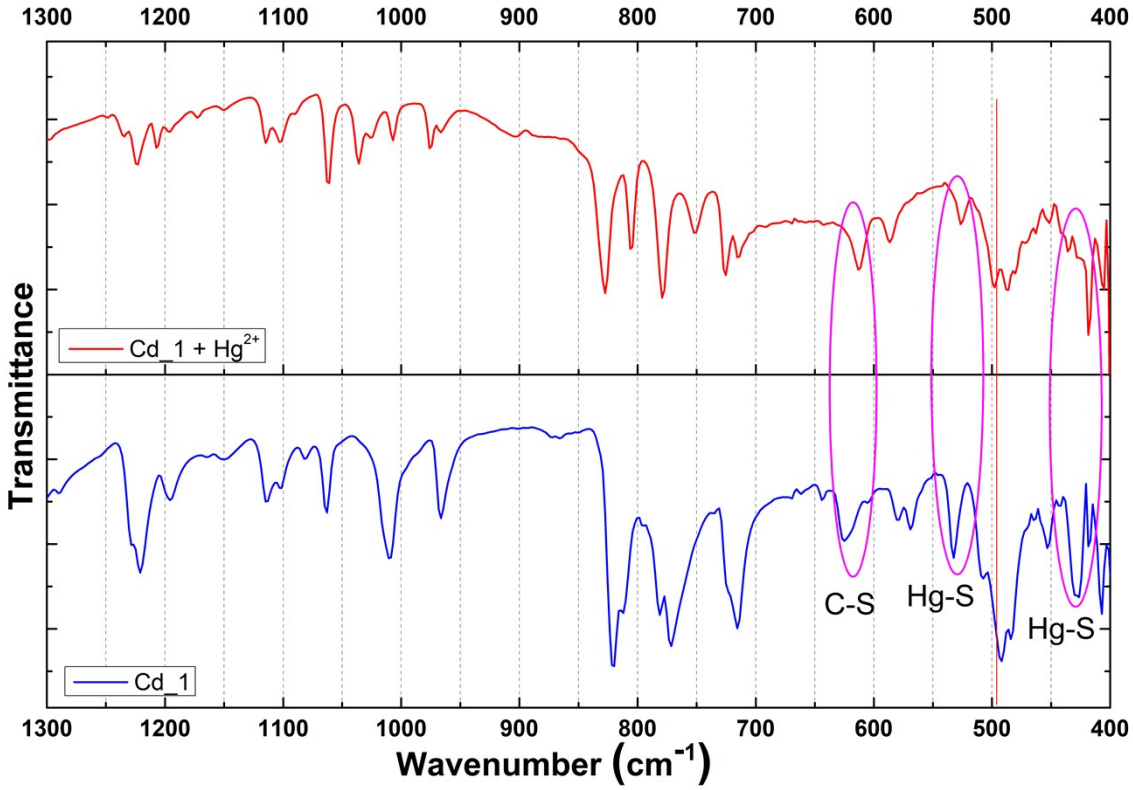

Fig. S28: Blue line shows the IR spectra of compound **1.** Red line shows the IR spectra of **Cd_1** after the addition Hg^{2+} ions. The encircled areas are a visual guide to point out the changes in IR peaks after the addition of Hg^{2+} ions.

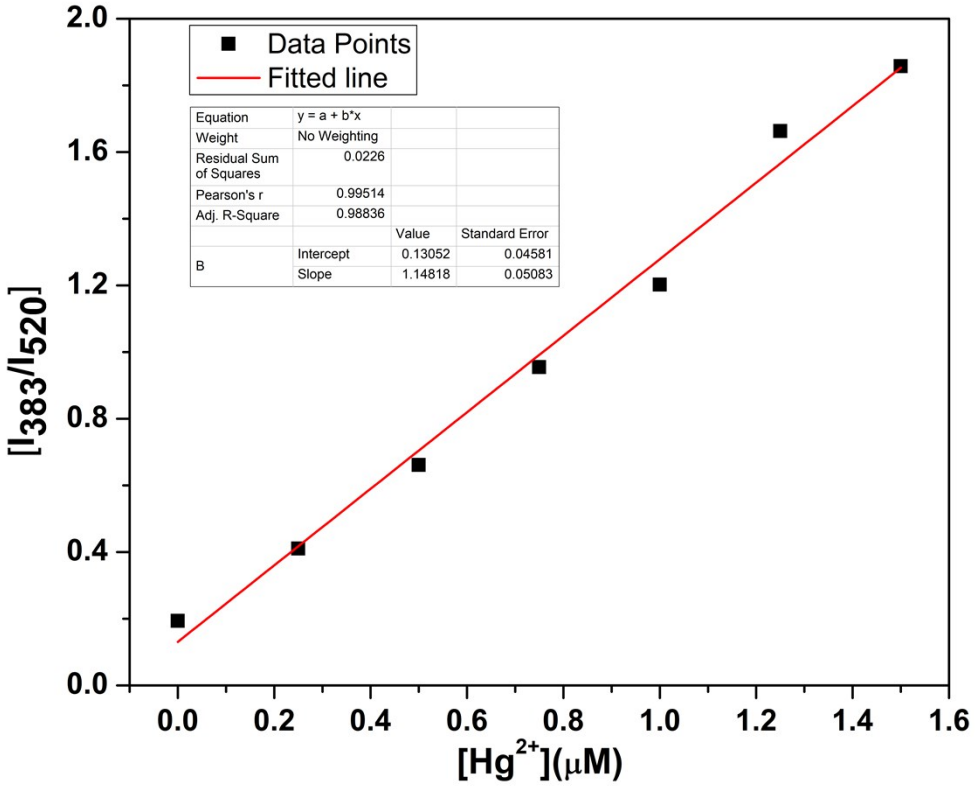

Fig. S29: Plot of ratio of luminescence intensity at 383 nm and 520 nm of compound **Cd_1** upon addition of Hg^{2+} in low concentration region. Red line is the linear fitted line of experimental data points (R^2 = 0.99514) and the slope of the graph is 1.148.

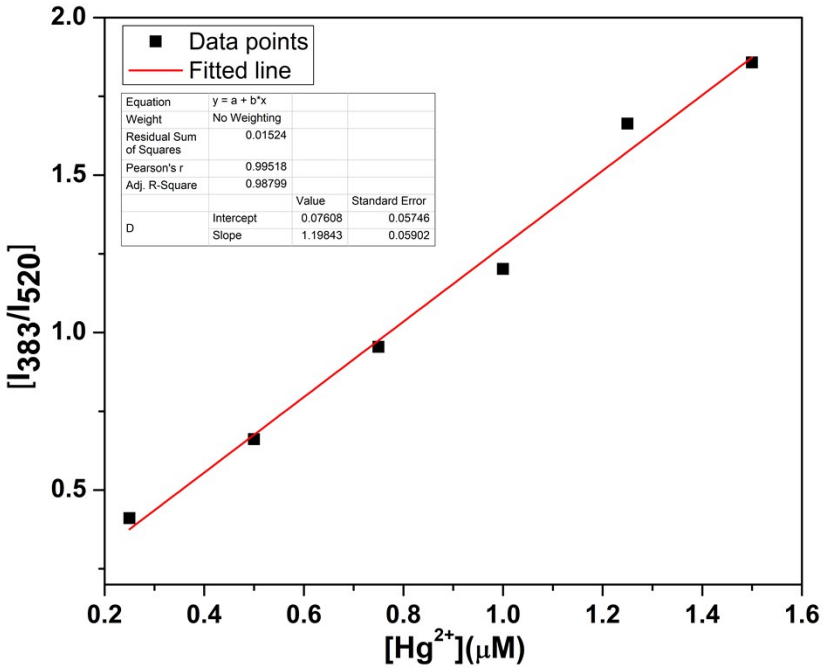

Fig. S30: Plot of ratio of luminescence intensity at 383 nm and 520 nm of compound **Cd_1** upon addition of Hg^{2+} in low concentration region. Red line is the linear fitted line of experimental data points (R^2 = 0.99518) and the slope of the graph is 1.198.

Calculation of Detection Limit

Standard deviation for compound Cd_1

Blank Reading (only compound **Cd_1**)	Fluorescence Intensity Ratio
Reading 1	0.10
Reading 2	0.12
Reading 3	0.13
Reading 4	0.12
Reading 5	0.14
Standard deviation(σ)	0.015

Standard Deviation (σ)	0.015
Slope from Graph (m)	1.20 μM^{-1}

Thus, Limit of Detection (LOD) = $3\sigma/m$ = (3×0.015)/1.20 = 37.5 nM = 7.4 ppb

Table S3: Summary of some reported metal-organic compounds for the detection of Hg^{2+} in an aqueous medium.

Sl. No	Sensor	K_{SV} (M^{-1})	Detection Limit	Luminescence response	Ref.
1	$[Cd(2\text{-}NH_2bdc)\ (tib)\cdot 4H_2O\cdot 0.5DMA]_n$	13×10^5	42 nM	Quenching	s1
2	Ad/Tb/DPA	NA	0.2 nM	Enhancement	s2
3	$\{[Cd_{1.5}(C_{18}H_{10}O_{10})]\cdot(H_3O)(H_2O)_3\}_n$	4.3×10^3	2 nM	Ratiometric	s3
4	Tb-CIP/AMP	NA	0.16 nM	Quenching	s4
5	$TbL_{1.5}(H_2O)_2]\cdot H_2O$	7.4×10^3	NA	Quenching	s5
6	$Zr_6O_4(OH)_4(TCPP)_{1.5}$	6.4×10^5	6 nM	Quenching	s6
7	Eu/IPA-Im	NA	2 nM	Enhancement	s7
8	$[Zn(\mu_2\text{-}1H\text{-}ade)(\mu_2\text{-}SO_4)]_n$	7.7×10^3	70 nM	Quenching	s8
9	Zn-based MOF	3737	1.8 μM	Enhancement	s9
10	$Ln(TATAB)\cdot(DMF)_4(H_2O)(MeOH)_{0.5}$	4851	4.4 nM	Quenching	s10
11	$\{[Zn(4,4'\text{-}AP)(5\text{-}AIA)].\ (DMF)_{0.5}\}_n$	1.01×10^9	9.9 pM	Quenching	s11
12	$[Pb_2(2\text{-}NCP)_2(L_1)]_n$	4.28×10^5	1.3 ppm	Quenching	s12
13	$[Cd(C_5N_1S_1H_4)(C_6O_5H_3)]$	1.15×10^6	37.5 nM	Ratiometric	This work

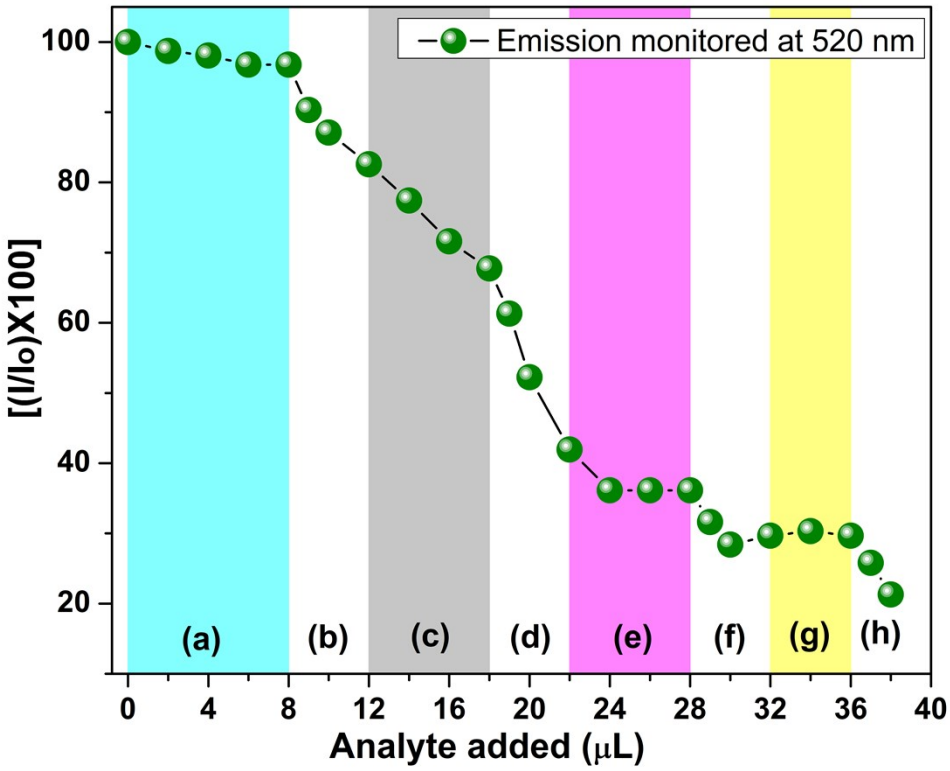

Fig. S31: Change of percentage in luminescence intensity at 520 nm upon the addition of 2 ***μ***L 1 mM quenchable metal ions followed by the addition of Hg^{2+} solution (two steps, 1 μL + 1 μL) and so on. The shaded portion represents the addition of Hg^{2+} in two steps. The added solution of metal ions are as below: (a) blank + 2 μL Fe^{3+} + 2 μL Cr^{3+} + 2 μL Al^{3+} + 2 μL Pb^{2+}, (b) a + 2 μL Hg^{2+}, (c) b + 2 μL Zn^{2+} + 2 μL Cd^{2+} + 2 μL Ag^{+} + 2 μL Cu^{2+}, (d) c + 2 μL Hg^{2+} (e) d + 2 μL Mn^{2+} + 2 μL Fe^{2+} + 2 μL Co^{2+} + 2 μL Ni^{2+}, (f) e + 2 μL Hg^{2+} (g) f + 2 μL Mg^{2+} + 2 μL K^{+} + 2 μL Na^{+}, (h) a + 2 μL Hg^{2+}.

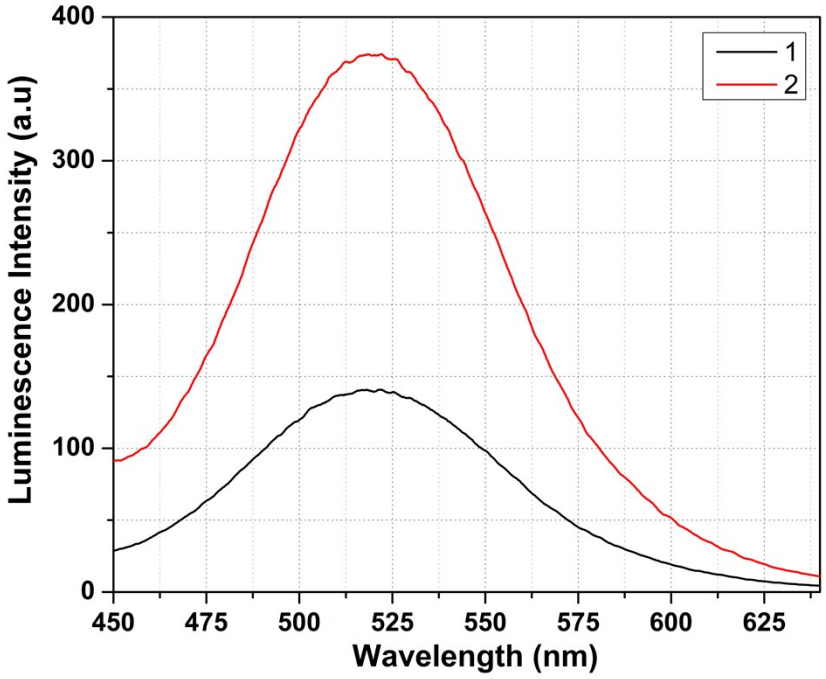

Fig. S32: (1) Luminescence spectrum of compound **Cd_1** (2) luminescence spectrum of compound **Cd_1** after passing Argon gas for 10 minutes upon excitation at 330 nm.

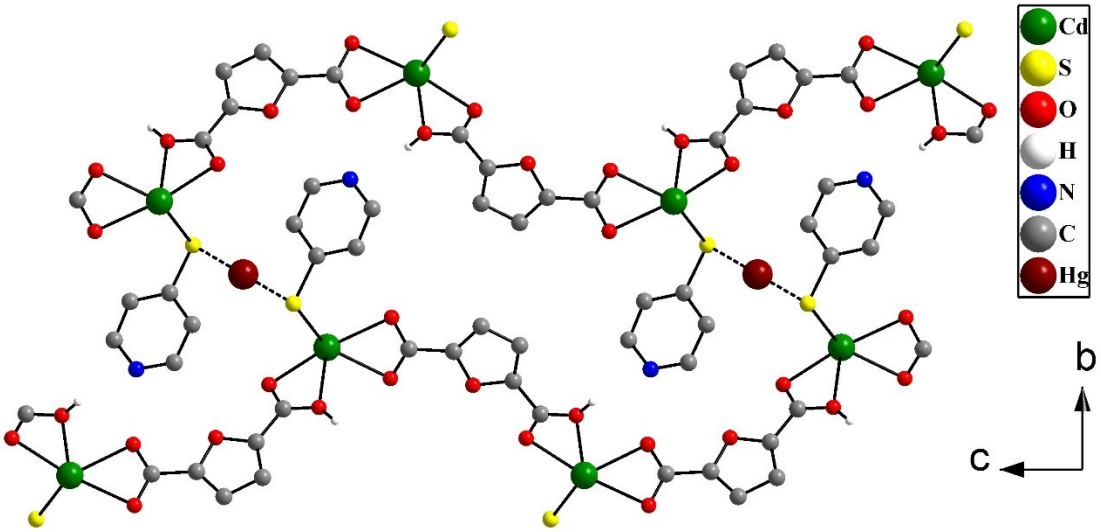

Fig. S33: Possible interactions between Hg^{2+} ions and **Cd_1** with two S atoms of the 4MPy moiety of two adjacent 1D chain.

REFERENCES

S1. Wen, L.; Zheng, X.; Lv, K.; Wang, C.; Xu, X., Two amino-decorated metal–organic frameworks for highly selective and quantitatively sensing of HgII and CrVI in aqueous solution. *Inorg. Chem.* **2015,** *54* (15), 7133-7135.

S2. Tan, H.; Liu, B.; Chen, Y., Lanthanide coordination polymer nanoparticles for sensing of mercury (II) by photoinduced electron transfer. *ACS nano* **2012,** *6* (12), 10505-10511.

S3. Wu, P.; Liu, Y.; Liu, Y.; Wang, J.; Li, Y.; Liu, W.; Wang, J., Cadmium-Based Metal–Organic Framework as a Highly Selective and Sensitive Ratiometric Luminescent Sensor for Mercury(II). *Inorg. Chem.* **2015,** *54* (23), 11046-11048.

S4. Liu, B.; Huang, Y.; Zhu, X.; Hao, Y.; Ding, Y.; Wei, W.; Wang, Q.; Qu, P.; Xu, M., Smart lanthanide coordination polymer fluorescence probe for mercury (II) determination. *Anal. Chim. Acta* **2016,** *912*, 139-145.

S5. Zhu, Y.-M.; Zeng, C.-H.; Chu, T.-S.; Wang, H.-M.; Yang, Y.-Y.; Tong, Y.-X.; Su, C.-Y.; Wong, W.-T., A novel highly luminescent LnMOF film: a convenient sensor for Hg2+ detecting. *J. Mater. Chem. A* **2013,** *1* (37), 11312-11319.

S6. Yang, J.; Wang, Z.; Li, Y.; Zhuang, Q.; Zhao, W.; Gu, J., Porphyrinic MOFs for reversible fluorescent and colorimetric sensing of mercury (II) ions in aqueous phase. *RSC Adv.* **2016,** *6* (74), 69807-69814.

S7. Li, Q.; Wang, C.; Tan, H.; Tang, G.; Gao, J.; Chen, C.-H., A turn on fluorescent sensor based on lanthanide coordination polymer nanoparticles for the detection of mercury (II) in biological fluids. *RSC Adv.* **2016,** *6* (22), 17811-17817.

S8. Rachuri, Y.; Parmar, B.; Bisht, K. K.; Suresh, E., Multiresponsive adenine-based luminescent Zn (II) coordination polymer for detection of Hg2+ and trinitrophenol in aqueous media. *Cryst. Growth Des.* **2017,** *17* (3), 1363-1372.

S9. Razavi, S. A. A.; Masoomi, M. Y.; Morsali, A., Double Solvent Sensing Method for Improving Sensitivity and Accuracy of Hg(II) Detection Based on Different Signal Transduction of a Tetrazine-Functionalized Pillared Metal–Organic Framework. *Inorg. Chem.* **2017,** *56* (16), 9646-9652.

S10. Xia, T.; Song, T.; Zhang, G.; Cui, Y.; Yang, Y.; Wang, Z.; Qian, G., A Terbium Metal–Organic Framework for Highly Selective and Sensitive Luminescence Sensing of Hg2+ Ions in Aqueous Solution. *Chem. Eur. J.* **2016,** *22* (51), 18429-18434.

S11. Pankajakshan, A.; Kuznetsov, D.; Mandal, S., Ultrasensitive Detection of Hg(II) Ions in Aqueous Medium Using Zinc-Based Metal–Organic Framework. *Inorg. Chem.* **2019,** *58* (2), 1377-1381.

S12. Qiao, Y.; Guo, J.; Li, D.; Li, H.; Xue, X.; Jiang, W.; Che, G.; Guan, W., Fluorescent sensing response of metal-organic frameworks for the highly sensitive detection of Hg2+ and nitrobenzene in aqueous media. *J. Solid State Chem.* **2020,** *290*, 121610.